

Modeling Steel Corrosion in Concrete Structures - Part 2: A Unified Adaptive Finite Element Model for Simulation of Steel Corrosion

Luc The Ngoc Dao^{1,}, Vinh The Ngoc Dao², Sang-Hyo Kim¹ and Ki Yong Ann¹*

¹ School of Civil and Environmental Engineering, Yonsei University, Seoul 120-749, Republic of Korea

² School of Civil Engineering, The University of Queensland, Australia

*E-mail: lucdao@yonsei.ac.kr

Received: 6 January 2010 / *Accepted:* 15 March 2010 / *Published:* 31 March 2010

Recently, numerical methods that can reliably predict the service life of reinforced concrete structures have attracted increasing attention. In this, the second of two companion papers, relevant literature on numerical modeling of steel corrosion is first reviewed. Then, a unified and straight-forward algorithm that is capable of performing different types of steel corrosion modeling using a single scheme is presented, based on the new inverse relation relating the current density with potential for the cathodic reaction proposed in the companion paper. Besides being significantly more efficient computationally arising from the selective mesh refinement feature of adaptive finite element modeling, the proposed algorithm can also efficiently model complex geometries and incorporate parameters that vary over the domain.

Keywords: Concrete, Corrosion, Numerical modeling, Adaptive FEM, Inverse relation

1. INTRODUCTION

Corrosion of steel reinforcement has been considered the most prevalent form of deterioration of reinforced concrete structures, potentially seriously compromising the service life of these structures [1, 2]. Service life prediction and enhancement of concrete structures under corrosion attack are therefore of significant importance. In recent years, in addition to laborious experimental investigations, numerical methods that are capable of simulating the corrosion processes of reinforcing steel and thus reliably predict the service life of concrete structures have gained increasing attention [3-6].

The modeling of steel corrosion in concrete structures involves solving the governing equation in Laplace form that satisfies the two boundary conditions of potential and current density at the steel-concrete interface [7, 8]. Currently available models often adopt only one of the above two boundary conditions, with the other satisfied by iteration to convergence. This is principally due to the lack of a suitable inverse relation that relates the current density with potential for the cathodic reaction. In the companion paper [9], such an inverse relation is proposed, which enables the two boundary conditions to be combined and satisfied simultaneously. This paper aims to utilize the newly proposed inverse relation to develop a unified and straight-forward algorithm for modeling of steel corrosion in concrete structures.

2. KINETICS OF CORROSION

The kinetics of corrosion is presented in detail in the companion paper [9], and is summarized in Table 1 for convenient reference.

Table 1. Summary of the kinetics of steel corrosion in concrete structures.

		Anodic	Cathodic
Reaction		$Fe \rightarrow Fe^{2+} + 2e^-$	$O_2 + 2H_2O + 4e^- \rightarrow 4OH^-$
Polarization	Activation	$\eta_a = \beta_a \log \frac{i_a}{i_{a0}}$	$\eta_{ca} = -\beta_c \log \frac{i_c}{i_{c0}}$
	Concentration		$\eta_{cc} = -\frac{2.303RT}{zF} \log \frac{i_L}{i_L - i_c}$
Stern and Geary relation for potential-current density relation [10, 11]		$\phi_a = \phi_{a0} + \eta_a$ $= \phi_{a0} + \beta_a \log \frac{i_a}{i_{a0}}$	$\phi_c = \phi_{c0} + \eta_{cc} + \eta_{ca}$ $= \phi_{c0} - \frac{2.303RT}{zF} \log \frac{i_L}{i_L - i_c} - \beta_c \log \frac{i_c}{i_{c0}}$

Note: η_a is the activation polarization of the anodes; η_{ca} and η_{cc} are the activation and concentration polarization of the cathodes; ϕ_a and ϕ_c are the polarized potential of the anodic and cathodic reaction; β_a and β_c are the Tafel slope of the anodic and cathodic reaction; i_a and i_c are the anodic and cathodic current density; i_{a0} and i_{c0} are the exchange current density of the anodic and cathodic reaction; i_L is the limiting current density of the cathodic reaction; R is the universal gas constant (8.314J/K.mol); T is the absolute temperature; F is Faraday's constant (9.65×10^4 C/mol); and z is the number of electrons exchanged in the cathodic reaction.

3. A UNIFIED FINITE ELEMENT MODEL FOR CORROSION SIMULATION

3.1. Governing equation and boundary conditions (BCs)

The modeling of steel reinforcement corrosion in concrete requires knowledge of the potential distribution around the reinforcement as well as in concrete. Assuming electrical charge conservation, the potential distribution can be represented by the Laplace's equation

$$\nabla^2 \phi = \frac{\partial^2 \phi}{\partial x^2} + \frac{\partial^2 \phi}{\partial y^2} = 0 \tag{1}$$

where ϕ is the electrical potential (V) and ∇^2 is the Laplacian operator. Calculating the potential distribution involves solving Eq. 1, subject to boundary conditions described below.

There are three types of boundaries, namely, the passive boundary, the active boundary and the boundary where no current density is allowed. While the protected passive layer remains and only cathodic reaction occurs on the passive boundary, the passive layer is destroyed and both anodic and cathodic reactions can happen on the active boundary. In this paper, the parameters related to the passive and active boundaries are denoted by a superscript p and a , respectively (e.g. ϕ^p , ϕ^a).

Based on reactions on active and passive boundaries, corrosion modeling can be classified as either macro-cell or macro-and-micro-cell modeling. (Micro-cell corrosion has been successfully modeled by using macro-cell model [12-14].) The boundary conditions corresponding to these two types of corrosion modeling are illustrated in Fig. 1 and detailed as follows.

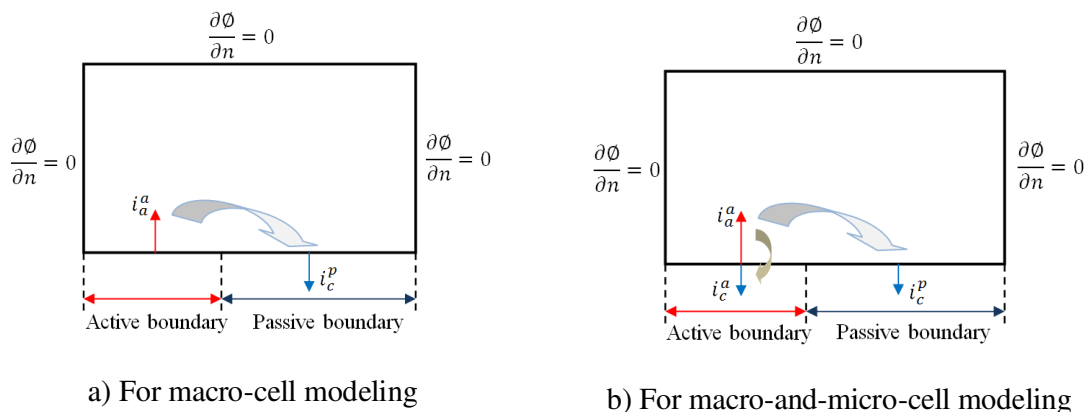


Figure 1. Boundary conditions for macro-cell and macro-and-micro-cell modeling.

Macro-cell corrosion modeling

In macro-cell corrosion modeling, no cathodic reaction happens on the active boundary [8, 12-16] and thus all the electrons produced by anodic reaction on the active boundary are consumed by cathodic reaction in the passive boundary. Table 2 summarizes the potential and current density conditions for different types of boundaries for this type of modeling.

Table 2. Boundary conditions for macro-cell corrosion modeling [8, 12-16].

Boundaries		Active	Passive	Other
Current density		$i = \frac{1}{r} \frac{\partial \phi}{\partial n}$	$i = \frac{1}{r} \frac{\partial \phi}{\partial n}$	$i = \frac{1}{r} \frac{\partial \phi}{\partial n} = 0$
Potential	Anodic reaction	$\phi^a = \phi_{a0} + \beta_a \log \frac{i_a}{i_{a0}}$		
	Cathodic reaction		$\phi^p = \phi_{c0} - \beta_c \log \frac{i_c^p}{i_{c0}} - \frac{2.303RT}{zF} \log \frac{i_L}{i_L - i_c^p}$	

Note: r is the electrical resistance of concrete and n is the direction normal to the steel surface.

Macro-and-micro-cell corrosion modeling

In macro-and-micro-cell modeling, cathodic reaction is considered on the active boundary [7]. As a result, the electrons generated by anodic reaction on the active boundary are consumed by cathodic reaction both on this boundary and on the passive boundary. The boundary conditions for the macro-and-micro-cell modeling are summarized in Table 3.

Table 3. Boundary conditions for macro-and-micro-cell corrosion modeling [7].

Boundaries		Active	Passive	Other
Current density		$i = \frac{1}{r} \frac{\partial \phi}{\partial n}$	$i = \frac{1}{r} \frac{\partial \phi}{\partial n}$	$i = \frac{1}{r} \frac{\partial \phi}{\partial n} = 0$
Potential	Anodic reaction	$\phi^a = \phi_{a0} + \beta_a \log \frac{i_a}{i_{a0}}$		
	Cathodic reaction	$\phi^a = \phi_{c0} - \beta_c \log \frac{i_c^a}{i_{c0}} - \frac{2.303RT}{zF} \log \frac{i_L}{i_L - i_c^a}$	$\phi^p = \phi_{c0} - \beta_c \log \frac{i_c^p}{i_{c0}} - \frac{2.303RT}{zF} \log \frac{i_L}{i_L - i_c^p}$	

It should be highlighted from Fig. 1 and the description above that the only difference between the two models is whether cathodic reaction in active boundaries is considered (i.e. in macro-and-micro-cell corrosion modeling) or not (i.e. in macro-cell corrosion modeling).

3.2. A unified concept for corrosion modeling

Currently available models often use either potential or current density as the boundary conditions when solving the governing equation, with the other condition satisfied by iteration to convergence. Unfortunately, this leads to different nonlinear schemes for different types of corrosion modeling. Specifically,

- In macro-cell modeling [8, 12-16]: The current densities are first determined from the potential distribution previously obtained using relevant relations in Table 2. The potentials

along the active and passive boundaries are then updated and subsequently adopted as prescribed BCs to solve the governing equation in the next iteration until convergence is attained.

- In macro-and-micro-cell modeling [7]: The current densities are first determined from the potential distribution previously obtained using relevant relations in Table 3. These current densities are then used as natural BCs to solve the governing equation in the next iteration until convergence is reached. It should be noted that, since only natural BCs are used, additional techniques are required to ensure unique solution.

It is thus highly desirable to satisfy the two boundary conditions of potential and current density simultaneously, which can be achieved only by suitable inverse relations relating the current density with potential for the cathodic reaction. In the companion paper [9], such an accurate yet simple relation has been proposed. Based on this newly proposed relation, the combined boundary conditions for different types of corrosion modeling can be derived and are given in Table 4.

Table 4. Combined conditions for the two types of corrosion modeling.

	Active boundary	Passive boundary	Other boundary
Macro-cell modeling	$\frac{\partial \phi}{\partial n} = ri_a^a$	$\frac{\partial \phi}{\partial n} = ri_c^p$	$\frac{\partial \phi}{\partial n} = 0$
Macro-and-micro-cell modeling	$\frac{\partial \phi}{\partial n} = r(i_a^a - i_c^a)$	$\frac{\partial \phi}{\partial n} = ri_c^p$	$\frac{\partial \phi}{\partial n} = 0$

where

$$i_a^a = i_{a0} e^{\frac{2.303(\phi^a - \phi_{a0})}{\beta_a}} \tag{2}$$

$$i_c^a = \left(\frac{\left(i_{c0} e^{\frac{2.303(\phi_{c0} - \phi^a)}{\beta_c}} \right)^3}{1 + \left(\frac{i_{c0} e^{\frac{2.303(\phi_{c0} - \phi^a)}{\beta_c}}}{i_L} \right)^3} \right)^{\frac{1}{3}} \tag{3}$$

$$i_c^p = \left(\frac{\left(i_{c0} e^{\frac{2.303(\phi_{c0} - \phi^p)}{\beta_c}} \right)^3}{1 + \left(\frac{i_{c0} e^{\frac{2.303(\phi_{c0} - \phi^p)}{\beta_c}}}{i_L} \right)^3} \right)^{\frac{1}{3}} \tag{4}$$

Besides the enabling of the two boundary conditions of potential and current density to be satisfied simultaneously, the adoption of combined conditions (Table 4) as mixed BCs for solving the governing equation also offers several other advantages. Specifically,

- The two types of corrosion modeling can now be conveniently solved by a single scheme. Macro-cell modeling clearly is just a specific case of macro-and-micro-cell modeling when the cathodic reaction in active area is absent (i.e. $i_c^a = 0$) (Table 4).
- The unique solution is obtained automatically.
- Advanced finite element methods (e.g. Adaptive FEM), which can significantly enhance the efficiency and accuracy of the analysis, are also more efficiently implemented.

3.3. Adaptive FEM for corrosion modelling

In order to solve the governing equation (Eq. 1) for cases with nonlinear boundary conditions (Table 2-4), numerical methods are required. Table 5 summarizes currently available numerical methods for corrosion modeling and their major limitations.

Table 5. Summary of available numerical methods.

<i>Numerical methods</i>	<i>Limitations</i>
Finite different method (FDM) [4, 17]	The geometries need to be conformed with coordinate systems, and hence complicated geometries and boundaries cannot be accommodated.
Finite element method (FEM) [7, 8, 15, 16, 18, 19]	Due to localized strong gradients at points of transition from active to passive areas, the uniform mesh has to be very dense, and hence high computational cost.
Boundary Element Method (BEM) [20-23]	Variations of concrete properties (e.g concrete resistivity) in one domain cannot be adequately simulated. In addition, the potential distribution in concrete cannot be directly determined.

A more advanced FEM, Adaptive FEM, that effectively overcomes all of the above limitations, offers a much better alternative. First, Adaptive FEM can simulate any geometry, including those with complex shapes and boundaries. Second, parameters that vary over the domain (e.g. concrete resistivity) as well as the potential distribution can be easily accommodated. Also, the selective mesh refinement feature of Adaptive FEM makes it computationally much more efficient than conventional FEM with uniform mesh. These are clearly demonstrated in a subsequent section on model verification.

Fig. 2 provides a schematic representation of the Adaptive FEM nonlinear algorithm for unified corrosion modeling. The input parameters include geometry- and kinetics- defining parameters, properties of concrete and oxygen concentration. The estimation of Root-Mean-Square errors in flux for each element and the local mesh refinement algorithm are of significant importance. However, due to the scope of the paper, further related details are not provided herein. The typical resulting outputs,

among others, are (1) potential distribution on the boundaries as well as over the whole domain; (2) current densities on the active and passive boundaries and their average values (The anodic current density is also the corrosion current density); and (3) corrosion products, corrosion depth as well as corrosion product expansion developed at steel surface with time.

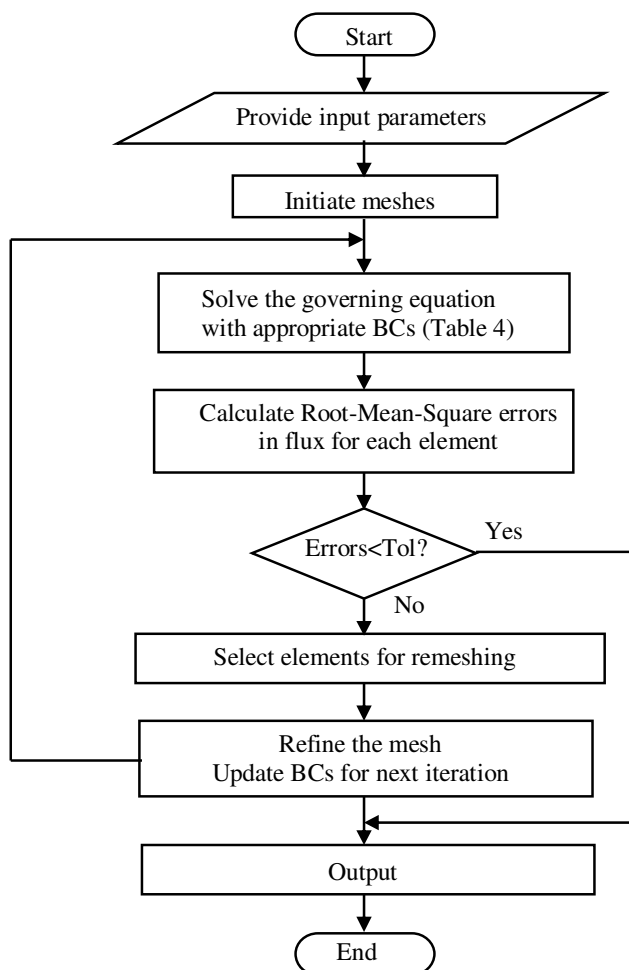


Figure 2. Nonlinear algorithm for unified corrosion modeling.

4. MODEL VERIFICATION

The validity and capability of the proposed model is now evaluated through two case studies. While the first case study validates the model against published results obtained from an investigation based on a macro-cell modeling [15], the second case study evaluates the model against results of another investigation based on a macro-and-micro-cell modeling [7]. The input parameters are summarized in Table 6.

Table 6. Summary of input parameters.

Parameters	Unit	Ge and Isgor 2007 [15]	Kim and Kim 2008 [7]
Length	mm	300	110
Height	mm	100	170
Equilibrium potential for anodic reaction ϕ_{a0}	mV vs. SCE	-780	-690
Exchange current density for anodic reaction i_{a0}	A/mm ²	187.5×10^{-12}	275×10^{-12}
Tafel slope for anodic reaction β_a	mV/dec	60	90.7
Equilibrium potential for cathodic reaction ϕ_{c0}	mV vs. SCE	160	160
Exchange current density for cathodic reaction i_{c0}	A/mm ²	6.25×10^{-12}	6×10^{-12}
Tafel slope for cathodic reaction β_c	mV/dec	160	176.3
Limiting current density i_L	A/mm ²	1×10^{-6}	
Concrete resistivity	Ohm.mm	140,000	150,000

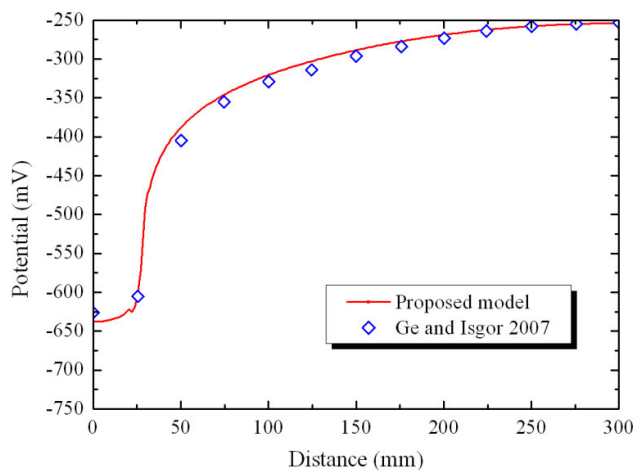
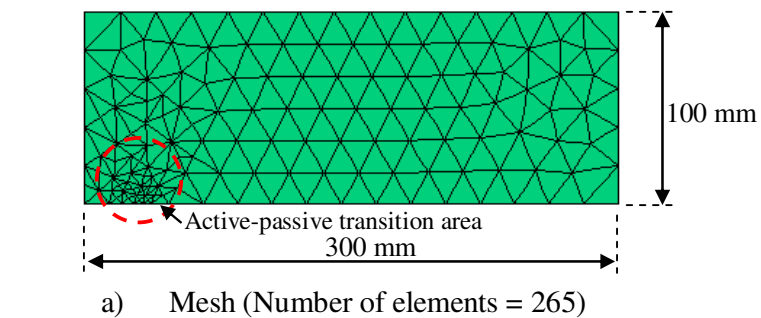
4.1. Verification with results from macro-cell modeling

In this part, results from the proposed model are compared with those based on macro-cell modeling [15]. The comparison is carried out for two anode-to-cathode ratios of 0.1 and 1: the former for the lengths of the active and passive boundaries of about 27.3 mm and 272.7 mm, respectively; and the latter for the lengths of both the active and passive boundaries of 150 mm. The resulting potential and current density distributions obtained from the proposed model, together with those from [15], are plotted in Fig. 3 and Fig. 4. It can be observed that, for both cases, the two models give very similar results, confirming the validity of the proposed model. Importantly, the proposed model requires only about 260 elements, which is remarkably smaller than the 1200 uniform-meshing elements used in [15]. This is a direct result of the selective mesh refinement feature discussed earlier of Adaptive FEM, in which finer mesh is generated in the active-passive transition areas and coarser mesh elsewhere. Adaptive FEM is thus computationally much more efficient than conventional FEM with uniform meshing.

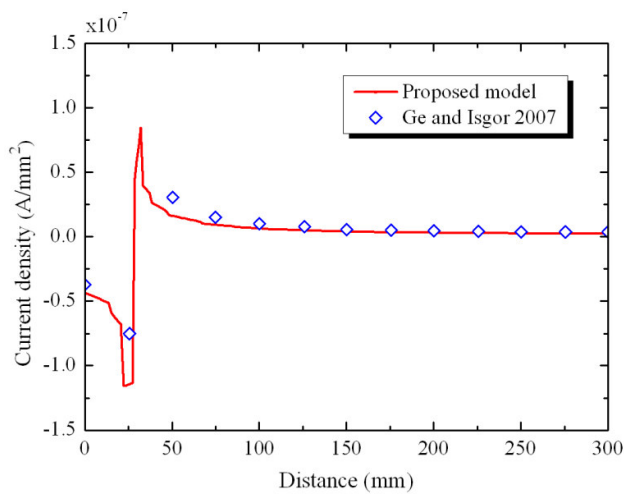
4.2. Verification with results from macro-and-micro-cell modeling

In this part, results of the proposed model are compared with those based on a macro-and-micro-cell modeling [7]. Fig. 5a represents the finite element meshes constructed for the corrosion analysis by the two models of a concrete specimen with 20 mm-in-diameter steel reinforcement spacing at 200 mm and concrete cover of 50 mm. It should be pointed out that although desirable denser meshes around the steel surface are generated in both cases, such an effect is achieved automatically in the proposed model without resorting to additional specific inputs in [7].

The resulting distributions of corrosion potential are presented in Fig. 5b. It can be readily observed that the two models provide essentially very similar results, further confirming the validity of the proposed model.

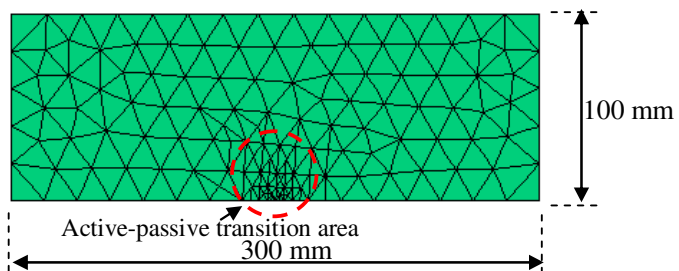


a) Potential distribution

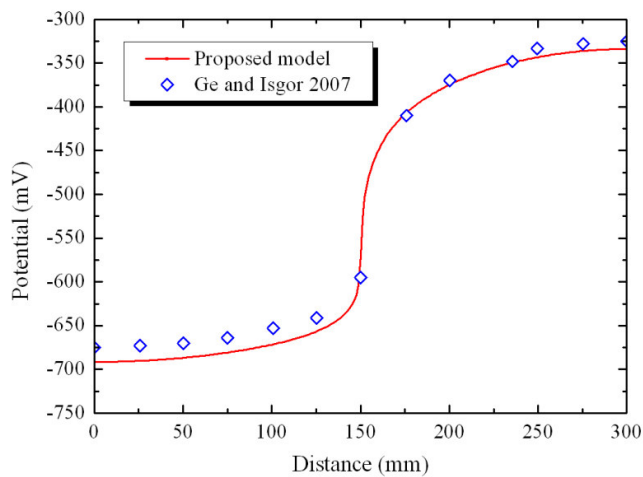


b) Current density distribution

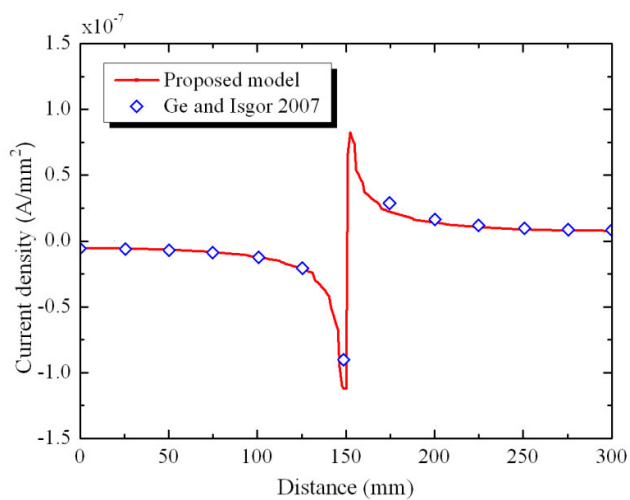
Figure 3. Comparison of results for anode-to-cathode ratio of 0.1.



a) Mesh (Number of elements = 258)



b) Potential distribution



c) Current density distribution

Figure 4. Comparison of results for anode-to-cathode ratio of 1.

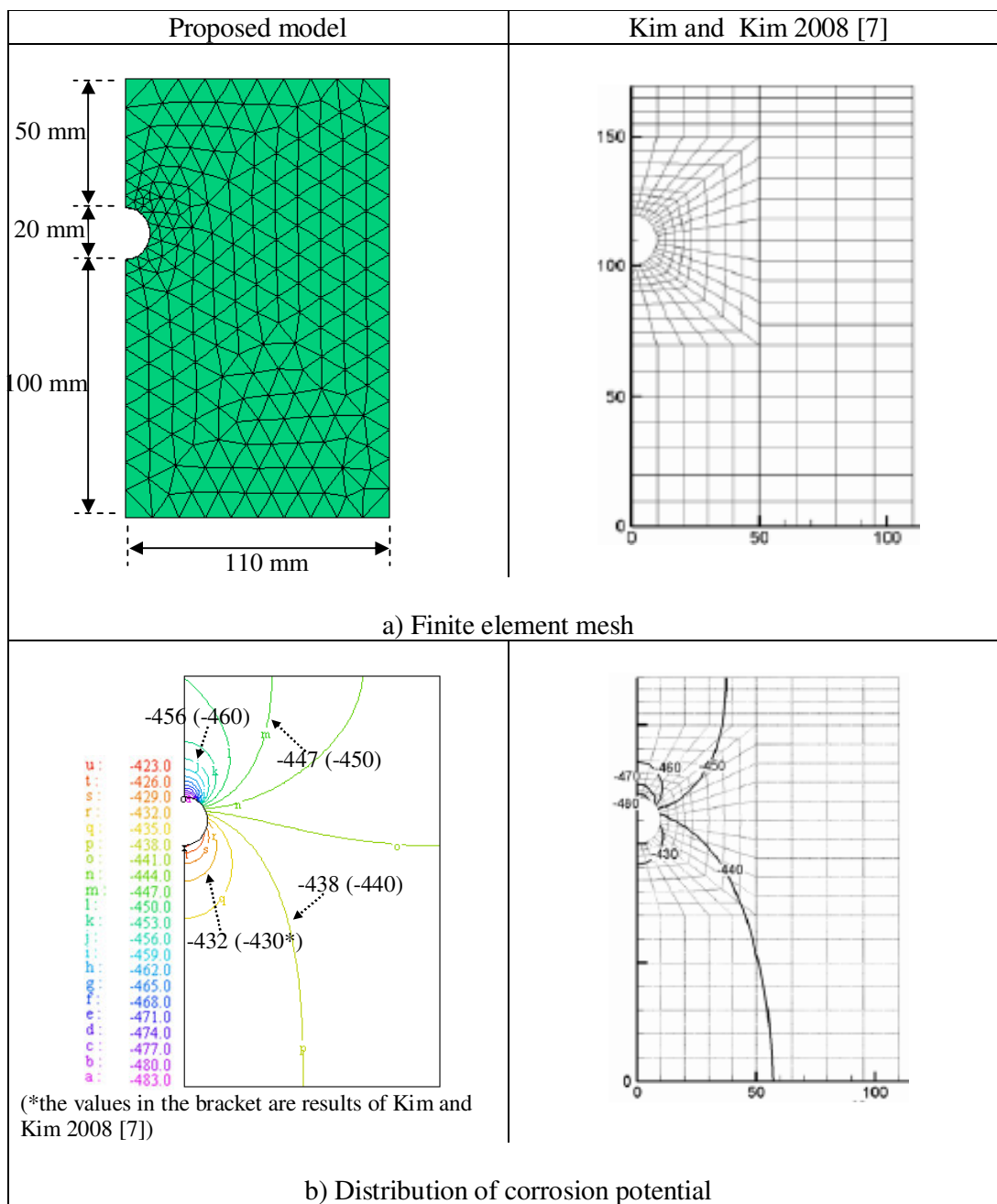


Figure 5. Results from macro-and-micro-cell modeling.

The two case studies above have clearly demonstrated the capability of the proposed unified adaptive FEM model for simulation of steel corrosion. The proposed model has also been successfully incorporated into a more generalized model for steel corrosion in concrete structures, including localized corrosion, localized cover cracking as well as service life prediction of concrete structures under corrosion attack. These will be presented in future publications.

5. CONCLUSIONS

In this paper, after a critical review of relevant literature on numerical modeling of steel corrosion, a unified algorithm that is capable of performing different types of steel corrosion modeling using a single scheme has been proposed. In addition, adaptive FEM, which effectively overcomes most major limitations of currently available numerical methods for corrosion modeling, has also been incorporated in the proposed algorithm.

Through two case studies, the validity and capability of the proposed algorithm has been clearly demonstrated. Besides being significantly more efficient computationally arising from the selective mesh refinement feature of Adaptive FEM, the proposed unified algorithm for simulation of steel corrosion can also efficiently model complex geometry and incorporate parameters that vary over the domain (e.g. concrete resistivity) as well as the potential distribution.

ACKNOWLEDGEMENTS

The authors would like to thank Concrete Corea for the support in finance for this research. Mr L.T.N. Dao specially thanks Prof H.W. Song for his sincere support and valuable advice in setting up this study.

References

1. S.L. Amey, D.A. Johnson, M.A. Miltenberger and H.Farzam, *ACI Structural Journal*, 95 (2) (1998) 205.
2. K.Y. Ann and H.-W. Song, *Corrosion Science*, 49 (11) (2007) 4113.
3. J. Gulikers, *Corrosion in reinforced concrete structures*, CRC Press (2005) 71.
4. S.C. Kranc and A.A. Sagüés, *Corrosion Science*, 43 (7) (2001) 1355.
5. H.-W. Song, H.-J. Kim, V. Saraswathy and T.-H. Kim, *Int. J. Electrochem. Sci.*, 2 (2007) 341.
6. R.R. Hussain and T. Ishida, *Int. J. Electrochem. Sci.*, 4 (2009) 1178.
7. C.-Y. Kim and J.-K. Kim, *Construction and Building Materials*, 22 (6) (2008) 1129.
8. O.B. Isgor and A.G. Razaqpur, *Materials and Structures*, 39 (3) (2006) 291.
9. L.T.N. Dao, V.T.N. Dao, S.-H. Kim and K.Y. Ann, *Int. J. Electrochem. Sci.*, 5 (2010).
10. H.H. Uhlig and R.W. Revie, *Corrosion and corrosion control: an introduction to corrosion science and engineering*, John Willey and Sons (2008).
11. M.G. Fontana, *Corrosion Engineering*, McGraw-Hill (1985).
12. P. Ghods, O.B. Isgor and M. Pour-Ghaz, *Materials and Corrosion*, 58 (4) (2007) 265.
13. M. Pour-Ghaz, O.B. Isgor and P. Ghods, *Corrosion Science*, 51 (2) (2009) 426.
14. M. Pour-Ghaz, O.B. Isgor and P. Ghods, *Corrosion Science*, 51 (2) (2009) 415.
15. J. Ge and O.B. Isgor, *Materials and Corrosion*, 58 (8) (2007) 573.
16. O.B. Isgor and A.G. Razaqpur, *Canadian Journal of Civil Engineering*, 33 (2006) 707.
17. S.C. Kranc and A.A. Sagues, *Journal of The Electrochemical Society*, 144 (8) (1997) 2643.
18. R. Montoya, O. Rendón and J. Genesca, *Materials and Corrosion*, 56 (6) (2005) 404.
19. E. Redaelli, L. Bertolini, W. Peelen and R. Polder, *Materials and Corrosion*, 57 (8) (2006) 628.
20. S. Jaggi, H. Bohni and B. Elsener, *Macrocell corrosion of steel in concrete - Experiments and Numerical modelling in The European Corrosion Congress*, Riva del Garda, Italy (2001).
21. J. Warkus, M. Brem and M. Raupach, *Materials and Corrosion*, 57 (8) (2006) 636.

22. J. Warkus and M. Raupach, *Materials and Corrosion*, 57 (12) (2006) 920.
23. J. Warkus and M. Raupach, *Materials and Corrosion*, 59 (2) (2008) 122.

© 2010 by ESG (www.electrochemsci.org)